Original Article

Assessing the histopathological features of rectal adenocarcinoma with chemical shift–encoded sequence (CSE)-MRI and diffusion-weighted imaging (DWI)

Yang Peng[1], Jiali Li[1], Xuemei Hu[1], Yaqi Shen[1], Daoyu Hu[1], Zhen Li[1], Ihab Kamel[2]

[1]Department of Radiology, Tongji Hospital, Tongji Medical College, Huazhong University of Science and Technology, Wuhan, China; [2]Russell H. Morgan Department of Radiology and Radiological Science, the Johns Hopkins Medical Institutions, Baltimore, MD, USA

Contributions: (I) Conception and design: Y Peng; (II) Administrative support: D Hu, Z Li; (III) Provision of study materials or patients: J Li; (IV) Collection and assembly of data: X Hu; (V) Data analysis and interpretation: Y Shen, I Kamel; (VI) Manuscript writing: All authors; (VII) Final approval of manuscript: All authors.

Correspondence to: Zhen Li, MD, PhD. Department of Radiology, Tongji Hospital, Tongji Medical College, Huazhong University of Science and Technology, 1095 Jiefang Avenue, Wuhan, Hubei 430030, China. Email: zhenli@hust.edu.cn.

Background: It is of clinical importance to assess the histopathological features of rectal cancer. The adipose tissue microenvironment is closely associated with tumor formation and progression. The chemical shift–encoded magnetic resonance imaging (CSE-MRI) sequence can noninvasively quantify adipose tissue. In this study, we aimed to investigate the feasibility of using CSE-MRI and diffusion-weighted imaging (DWI) to predict the histopathological features of rectal adenocarcinoma.

Methods: In this retrospective study, 84 patients with rectal adenocarcinoma and 30 healthy controls were consecutively enrolled at the Tongji Hospital of Tongji Medical College of Huazhong University of Science and Technology. CSE-MRI and DWI sequences were performed. The intratumoral proton density fat fraction (PDFF) and R2* of rectal tumors and normal rectal walls were measured. The histopathological features, including pathological T/N stage, tumor grade, mesorectum fascia (MRF) involvement, and extramural venous invasion (EMVI) status were analyzed. The Mann-Whitney test, Spearman correlation, and receiver operating characteristic (ROC) curves were used for statistical analyses.

Results: Patients with rectal adenocarcinoma demonstrated significantly lower PDFF and R2* values than did the control participants (5.35%±1.70% *vs.* 11.55%±3.41%, P<0.001; 35.60 s^{-1}±7.30 s^{-1} *vs.* 40.15 s^{-1}± 5.72 s^{-1}, P=0.003). PDFF and R2* were significantly different in the discrimination of T/N stage, tumor grade, and MRF/EMVI status (P=0.000–0.005). A significant difference was only noted in the differentiation of the T stage for the apparent diffusion coefficient (ADC) (1.09±0.26×10^{-3} mm^2/s *vs.* 1.00±0.11×10^{-3} mm^2/s; P=0.001). PDFF and R2* exhibited positive correlations with all the histopathological features (r=0.306–0.734; P=0.000–0.005), while ADC was negatively correlated with the T stage (r=–0.380; P<0.001). PDFF demonstrated diagnostic ability, with a sensitivity of 95.00% and a specificity of 87.50%, while R2* had a sensitivity of 95.00% and a specificity of 79.20% in differentiating T stage; both demonstrated a better diagnostic performance than did ADC.

Conclusions: Quantitative CSE-MRI imaging might serve as a noninvasive biomarker for assessing the histopathological features of rectal adenocarcinoma.

Keywords: Magnetic resonance imaging (MRI); rectal neoplasm; adipose tissue; pathology

Submitted Aug 22, 2022. Accepted for publication Mar 05, 2023. Published online Mar 27, 2023.
doi: 10.21037/qims-22-879
View this article at: https://dx.doi.org/10.21037/qims-22-879

Introduction

Colorectal cancer is one of the most common cancers globally and occurs in the alimentary tract. The majority of rectal cancer is adenocarcinoma, which accounts for 90% of all histological types. The treatment of rectal cancer is closely associated with preoperative histological features, such as tumor stage, lymph node status, histological differentiation, mesorectal fascia (MRF) invasion, and extramural vascular invasion (EMVI) (1-5). Therefore, accurate evaluation of prognosis-related histopathological features of rectal adenocarcinoma is essential for treatment planning.

The rectum is encapsulated by the surrounding mesorectum, which is rich in adipose tissue and has a close vascular and physical interface with visceral fat (6). A certain amount of adipose tissue is contained in the submucosal and serosal layers of the rectal wall. The adipose tissue secretes growth factors, hormones, and cytokines, which promote a favorable microenvironment for the potential pathogenesis of rectal cancer (7). The mutual interaction between rectal cancers and their peripheral adipose tissues could further facilitate the progression of rectal tumors (8). Reports have demonstrated that culture medium containing adipose tissue and adipocytes could enhance the proliferation of colon cancer cells (9). The adipokines and cytokines, secreted by adipocytes and accompanied by inflammatory cells, may also promote tumor development (10). Thus, we hypothesized that the intratumoral fat might directly affect the aggressiveness and progression of rectal adenocarcinoma, which might correlate with the histopathological features of tumors.

Magnetic resonance imaging (MRI) plays an important role in the assessment of rectal cancer. A functional MRI technique, namely iterative decomposition of water and fat with echo asymmetry and least squares estimation, can be used to noninvasively quantify the intratumoral fat content of rectal lesions. The chemical shift–encoded MRI (CSE-MRI) technique uses the multipoint Dixon method to steadily separate water and fat (11). This sequence employs an iterative least squares decomposition algorithm to measure the fat concentration based on the fat fraction map while correcting and adjusting for B0 field inhomogeneity and T1 and T2* effects (12). Furthermore, the reconstruction of water-only, fat-only, and R2* images are also produced simultaneously with fat fraction images in a single acquisition. CSE-MRI R2* values have been used to measure liver iron content (13) and tumor hypoxia of breast cancer (14), and R2* values have been previously reported to reflect the status of deoxyhemoglobin and blood oxygenation (15,16). However, to date, no investigation has been performed that uses the CSE-MRI technique to quantify intratumoral fat content and R2*-related biochemical changes of rectal adenocarcinoma.

Furthermore, diffusion-weighted imaging (DWI) is often used for the preoperative assessment of Tumor Node Metastasis (TNM) staging of rectal adenocarcinoma and is helpful for the discrimination of histological prognostic factors. However, DWI often fails to distinguish some histological features (17,18). Furthermore, previous studies suggest that apparent diffusion coefficient (ADC) measurements from DWI are not consistent with the utility of different *b* values (19-21). Moreover, DWI is based on echo planar imaging, which is susceptible to motion distortion, image blurring, and signal dropout (22). Therefore, the diagnostic value of DWI is limited.

Hence, the purpose of our study was to assess whether the histological features of rectal adenocarcinoma could be distinguished with the CSE-MRI sequence. We aimed to compare the ability of the CSE-MRI and DWI sequences to predict the histological features of rectal adenocarcinoma. We present the following article in accordance with the STARD reporting checklist (available at https://qims.amegroups.com/article/view/10.21037/qims-22-879/rc).

Methods

Study population

The study was conducted in accordance with the Declaration of Helsinki (as revised in 2013) and was approved by the Institutional Review Board of Tongji Hospital of Tongji Medical College of Huazhong University of Science and Technology; the requirement for written informed consent was waived due to the retrospective nature of the study. Between March 2016 and June 2020, the CSE-MRI sequence was performed on 127 patients who underwent a colectomy and had pathologically confirmed primary rectal adenocarcinoma. However, 43 patients were excluded due to the following reasons: they had pathologically proven mucinous adenocarcinoma (n=7), they had previously received rectal surgery or chemoradiotherapy before MR scanning (n=14), they had poor image quality of CSE-MRI images because of severe motion artifacts or intrarectal gas artifacts (n=6), the time interval between previous MR scanning and surgical operation surpassed

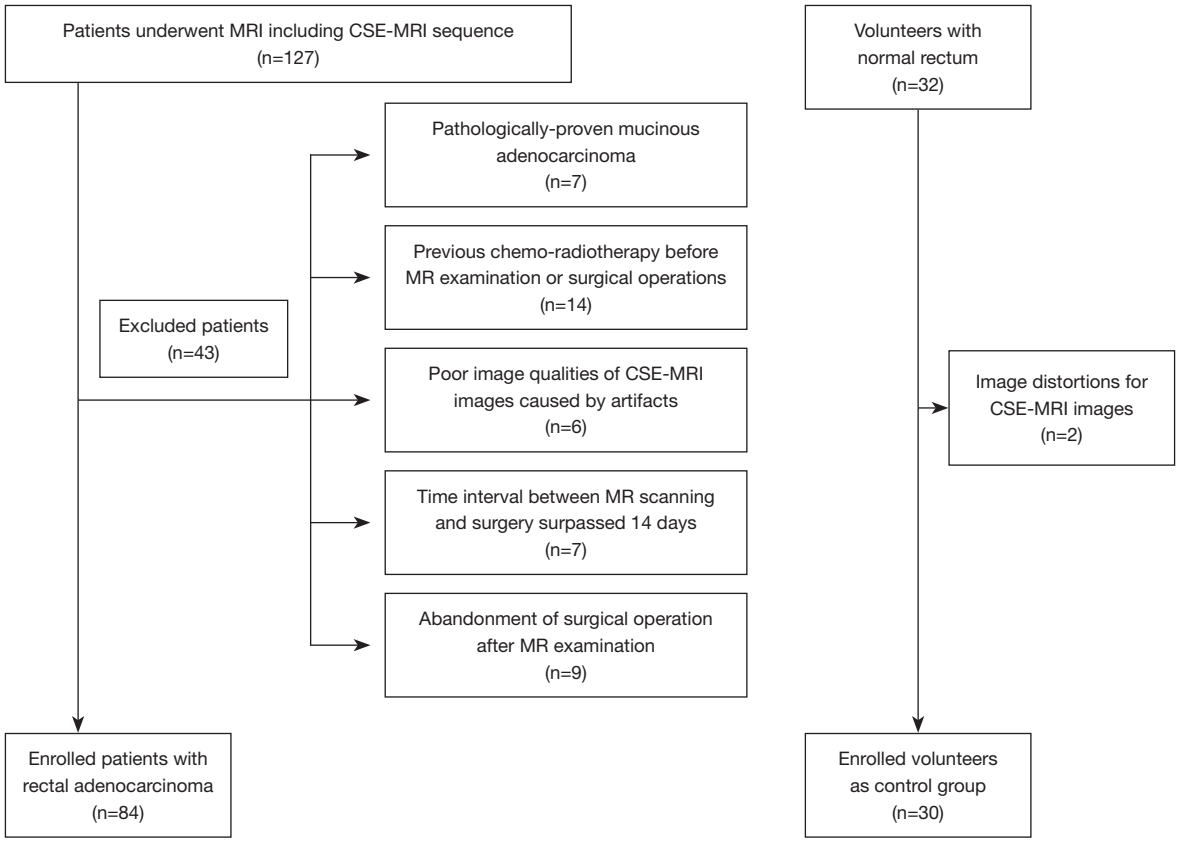

Figure 1 The flowchart for selection of patients. MRI, magnetic resonance imaging; CSE-MRI, chemical shift–encoded magnetic resonance imaging sequence.

14 days (n=7), and the surgical operation was abandoned after the MR examination (n=9; *Figure 1*). An additional 32 volunteers with normal rectums were enrolled in this study and were considered the control group. They underwent the same MR imaging protocol, including the CSE-MRI sequence. The control group had no previous history of gastrointestinal tumors, and MRI imaging confirmed the appearance of a normal rectum. Two volunteers were excluded from this study because image distortions made their CSE-MRI images difficult to diagnose (*Figure 1*).

MR imaging

MR examinations were performed using a 3.0 T MR imaging unit (Discovery MR750, GE Healthcare, Chicago, IL, USA) with a 32-channel phased-array torso coil. All patients were imaged in the supine position. A total of 5 mg of racanisodamine hydrochloride was administered intramuscularly to reduce bowel motion 30 minutes prior to MR scanning. All patients underwent a pelvic MR scan, and sequences included axial/sagittal T2-weighted imaging (T2WI), axial DWI, and axial CSE-MRI (*Table 1*). The axial T2WI, DWI, and CSE-MRI sequences were scanned perpendicularly to the long axis of the rectal tumor using sagittal T2WI as a reference.

Image analysis

The CSE-MRI proton density fat fraction (PDFF) maps and R2* maps, along with fat-phase, water-phase, in-phase, and out-phase reconstruction images generated using the post-processing software from the MR scanning machine, were directly transferred to the Picture Archiving and Communication System (PACS). The DWI images were transferred to a workstation (GE Advance Workstation 4.6) for ADC measurements. Two abdominal radiologists with 4 and 10 years of experience in diagnosing gastrointestinal diseases independently evaluated all the MR images. Both

Table 1 Parameters of CSE-MRI imaging, DWI, T2/T1-weighted imaging

Parameters	CSE-MRI	DWI	T2-weighted imaging	T1-weighted imaging
Sequence	GRE	EPI	FSE	FSE
Repetition time/echo time (ms)	5.9/2.6	4,000/75	5,629/85	500/11
Field of view (mm^2)	380×380	200×100	200×200	380×380
Matrix	160×160	128×64	448×314	320×224
Slice thickness (mm)	3.5	3	2	3
Flip angle (degree)	3°	N/A	111°	111°
b values (s/mm^2)	N/A	0, 800	N/A	N/A
NEX	0.5	12	4	2
Acquisition time (min:s)	0:19	2:32	4:04	1:44

CSE-MRI, chemical shift–encoded magnetic resonance imaging; DWI, diffusion-weighted imaging; GRE, gradient recalled echo; EPI, echo planar imaging; FSE, fast spin echo; NEX, number of excitations.

radiologists were blinded to the clinical information of patients and related pathological reports. The imaging data were anonymized and presented to the radiologists in a randomized order. Each radiologist drew free-hand regions of interest (ROIs) along the margin of the rectal lesions covering the whole tumors. T2WI and DWI were used as references for measurements of PDFF and R2*. Furthermore, T2-weighted images were also used as references for the quantification of ADC values. The ROIs were manually delineated on the largest section of every slice of rectal tumors on the PDFF, R2*, and DWI maps. Intraluminal gas, necrotic areas, cystic changes, hemorrhagic parts, and small vessels were avoided. The mean PDFF, R2*, and ADC values were obtained by averaging all the measurements based on the whole rectal lesions.

As for the control group, 5 free-hand ROIs were manually drawn on the normal rectum of each participant by the same 2 abdominal radiologists independently. Every single ROI encompassed the largest area of the randomized slice. The slices with intraluminal gas were eschewed for the possible artifacts caused by gas. The final averaged values of PDFF and R2* were calculated for the drawn areas.

Histopathologic assessment

All the histopathologic examinations were performed by a gastrointestinal pathologist with 15 years of experience. The pathologist was blinded to the clinical information and related imaging data. The resected specimens were first fixed with 10% formalin and then stained with hematoxylin and eosin (HE) after they were cut into 5-μm sections. The pathological results were presented in standard fashion and included the following histological features: TNM stage, histological differentiation, MRF, and EMVI status. In terms of degree of glandular formation, histological differentiation was classified into grade 1 (>95% gland formation, well differentiated), grade 2 (50–95% gland formation, moderately differentiated), and grade 3 (0–49% gland formation, poorly differentiated). In terms of the World Health Organization (WHO) criteria for tumor grade, grade 1 and 2 tumors were considered low-grade tumors, while grade 3 tumors were considered high grade. MRF involvement refers to tumors or malignant lymph nodes that are present within 1 mm of the MRF. EMVI is defined as the existence of tumor tissues or cells in the vascular structures beyond the muscularis propria layer of the rectum (23).

Statistical analysis

The values of PDFF, R2*, and ADC are expressed as mean ± standard deviation. The CSE-MRI and DWI parameters were tested for normality of data distributions using the Kolmogorov-Smirnov test. The interobserver agreement between the 2 radiologists on measurements of CSE-MRI and DWI parameters was analyzed using the interclass correlation coefficient (ICC) test. An ICC value of 0–0.20 indicated poor agreement, 0.21–0.40 fair agreement, 0.41–0.60 moderate agreement, 0.61–0.80 good agreement, and 0.81–1.00 excellent agreement.

The differences of PDFF, R2*, and ADC between T2,

T3, and T4 stages were assessed using the 1-way analysis of variance. Student *t* test or the Kruskal-Wallis test was used to evaluate the differences of the above parameters between N stage (N0 *vs.* N1–2), tumor grade (low grade *vs.* high grade), MRF status (negative *vs.* positive), and EMVI status (negative *vs.* positive). The association between MR parameters and histological features of rectal cancer was analyzed using the Spearman correlation coefficient. Furthermore, the differences in PDFF and R2* between the patient group and the control group were also analyzed using the Student test.

The diagnostic abilities of quantitative PDFF, R2*, and ADC in discriminating different histological features of rectal cancer were determined using receiver operating characteristic (ROC) curve analysis. The comparison of ROC curves for CSE-MRI and DWI parameters was analyzed using the DeLong test. The specificity, sensitivity, and Youden index were calculated. P values <0.05 referred to statistically significant results for all tests. SPSS 19.0 (IBM Corp., Armonk, NY, USA) and MedCalc software (Mariakerke, Belgium) were employed for statistical analyses.

Results

Our study cohort included 84 patients (56 males, 28 females; age range 30–82 years; median age 58 years) with rectal cancer and 30 volunteers (24 males, 6 females; age range 15–72 years; median age 43 years) in the control group with a normal rectum. The average tumor volume of those with rectal adenocarcinoma was 19.11±13.03 cm^3. The median time interval between conducting the MRI and histopathological assessment was 4 days (range, 3–6 days). No other clinical interventions were performed during this time interval. No adverse events from performing the MRI were witnessed.

Histopathological findings

Pathological TNM staging of rectal adenocarcinoma was extracted from corresponding pathological reports based on the eighth edition of the American Joint Committee on Cancer (AJCC) classification. A total of 24 tumors had invaded within the muscularis propria layer of the rectum (T2), 50 tumors extended beyond the muscularis propria into the perirectal tissues or mesorectum (T3), and 10 tumors encroached on the visceral peritoneum or adjacent organs/structures (T4). No metastatic lymph nodes were detected in 44 patients (N0), while 18 patients had no more than 3 metastatic lymph nodes (N1), and 22 patients had 4 or more metastatic lymph nodes (N2).

According to the WHO grading criteria, 25 tumors were classified as high grade (G3) and 59 tumors were classified as low grade, including 6 and 53 tumors that were classified as G1 and G2 tumors, respectively. Moreover, 53 patients had negative-EMVI status, while 31 patients had positive-EMVI status, and 62 patients had MRF-negative status, while 22 patients had MRF-positive status.

Comparison of PDFF and R2 between patients with rectal cancer and control participants*

The PDFF of patients with rectal cancer was significantly lower than that of control participants (5.35%±1.70% *vs.* 11.55%±3.41%; P<0.001). Significantly lower R2* values of patients with rectal cancer were found, as compared to those of control participants (35.60 ±7.30 *vs.* 40.15 ±5.72 s^{-1}; P=0.003).

Comparison of CSE-MRI and DWI between pathological T stage, N stage, histological differentiation, and MRF and EMVI status

The mean PDFF was significantly higher in rectal tumors with T3 and T4 staging (–6.17%±1.09% *vs.* 3.30%±1.12%, P<0.001), nodal involvement (6.43%±1.23% *vs.* 4.38%±1.48%, P<0.001), higher tumor grade (6.56%±1.46% *vs.* 4.84%±1.54%, P<0.001), and the positive MRF (6.63%±1.05% *vs.* 4.90%±1.66%, P<0.001) and EMVI status (6.58%±1.19% *vs.* 4.64%±1.54%, P<0.001) than in rectal tumors with T2 staging, nonmetastatic lymph nodes, a lower tumor grade, and negative MRF and EMVI status (*Table 2*). Furthermore, rectal adenocarcinoma with T3 and T4 staging (38.78 ±5.21 *vs.* 27.65 ±5.49 s^{-1}, P<0.001), lymph node involvement (39.19 ±5.87 *vs.* 32.34 ±6.98 s^{-1}, P=0.005), higher tumor grade (39.29 ±6.30 *vs.* 34.04 ±7.17 s^{-1}, P=0.003), and positive MRF (39.63 ±5.47 *vs.* 34.17 ±7.36 s^{-1}, P=0.002) and EMVI status (39.44 ±5.69 *vs.* 33.36 ±7.24 s^{-1}, P<0.001) demonstrated higher R2* values than did that with T2 staging nonmetastatic lymph node, a lower tumor grade, and negative MRF and EMVI status. As for ADC, it was statistically significant only for the discrimination of the T2 and T3+T4 stages [(1.09±0.26)×10^{-3} *vs.* (1.00±0.11)×10^{-3} mm^2/s; P=0.001]. No significant difference was noted in the assessment of other histological features (P>0.05; *Table 2*).

Table 2 CSE-MRI and DWI of different histological features of rectal adenocarcinoma

Factors	PDFF (%)		R2* (s^{-1})		ADC ($10^{-3}mm^2/s$)	
	Mean ± SD	P value	Mean ± SD	P value	Mean ± SD	P value
pT category						
T2 (n=24)	3.30±1.12	<0.001	27.65±5.49	< 0.001	1.09±0.26	0.001
T3 +T4 (n=60)	6.17±1.09		38.78±5.21		1.00±0.11	
pN category						
N0 (n=44)	4.38±1.48	<0.001	32.34±6.98	0.005	1.05±0.21	0.080
N1+N2 (n=40)	6.43±1.23		39.19±5.87		1.00±1.06	
Tumor grade						
G1+G2 (n=59)	4.84±1.54	<0.001	34.04±7.17	0.003	1.04±0.18	0.066
G3 (n=25)	6.56±1.46		39.29±6.30		0.98±0.12	
MRF						
Negative (n=62)	4.90±1.66	<0.001	34.17±7.36	0.002	1.03±0.18	0.600
Positive (n=22)	6.63±1.05		39.63±5.47		1.01±0.11	
EMVI						
Negative (n=53)	4.64±1.54	<0.001	33.36±7.24	< 0.001	1.04±0.19	0.102
Positive (n=31)	6.58±1.19		39.44±5.69		0.99±0.12	

SD, standard deviation. CSE-MRI, chemical shift–encoded magnetic resonance imaging; DWI, diffusion-weighted imaging; PDFF, proton density fat fraction; ADC, apparent diffusion coefficient; MRF, mesorectal fascia; EMVI, extramural vascular invasion.

Correlation of CSE-MRI and DWI with histological features of rectal adenocarcinoma

There was a significant positive correlation of mean PDFF to the T/N category, tumor grade, MRF status, and EMVI status of rectal cancer (r=0.467–0.734; all P values <0.001). Furthermore, mean R2* also exhibited a positive correlation with the above histological features of rectal adenocarcinoma (r=0.306–0.687; P=0.000–0.005). A negative correlation of ADC to T stage was observed (r=–0.380; P<0.001), but there were no other findings that suggested the association between ADC and other histological features (*Table 3*; *Figures 2*,*3*).

Diagnostic performance of CSE-MRI and DWI for distinguishing histological features of rectal adenocarcinoma

The areas under the curve (AUCs) for the discrimination of histological features of rectal adenocarcinoma ranged from 0.795–0.969 for PDFF, 0.693–0.938 for R2*, and 0.538–0.743 for ADC (*Table 4*). PDFF showed significantly higher diagnostic performance in distinguishing all the histopathological features than ADC except tumor grade (z=2.925–3.495; P=0.001–0.003). Significantly higher diagnostic abilities were noted for R2* than for ADC in distinguishing between the T and N stages of rectal adenocarcinoma (z=2.719, P=0.007; z=2.134, P=0.03). The diagnostic ability of PDFF in differentiating between the T2 and T3/T4 stages included a sensitivity of 95.00% and a specificity of 87.50%. The diagnostic ability of R2*in differentiating between T2 and T3/T4 stages included a sensitivity of 95.00% and a specificity of 79.20%. Both R2* and PDFF demonstrated a better diagnostic performance than did ADC (*Figure 4*).

Interobserver agreement

The ICC between the 2 readers was 0.996 (95% CI: 0.995–0.998) for PDFF, 0.996 (95% CI: 0.993–0.997) for R2*, and 0.998 (95% CI: 0.996–0.998) for ADC for patients with rectal adenocarcinoma. The interreader ICC was 0.996 (95% CI: 0.991–0.998) for PDFF and 0.989 (95% CI: 0.976–0.995) for R2* for control participants. These

Table 3 Correlations between CSE-MRI and DWI with different histological features of rectal adenocarcinoma

Histological features	PDFF (%)		R2* (s^{-1})		ADC (10^{-3} mm^2/s)	
	r value	P value	r value	P value	r value	P value
pT category	0.734	<0.001	0.687	<0.001	–0.380	<0.001
pN category	0.631	<0.001	0.487	<0.001	–0.192	0.080
Tumor grade	0.467	<0.001	0.306	0.005	–0.202	0.066
MRF	0.492	<0.001	0.324	0.003	–0.058	0.603
EMVI	0.560	<0.001	0.400	<0.001	–0.180	0.102

CSE-MRI, chemical shift–encoded magnetic resonance imaging; DWI, diffusion-weighted imaging; PDFF, proton density fat fraction; ADC, apparent diffusion coefficient; MRF, mesorectal fascia; EMVI, extramural vascular invasion.

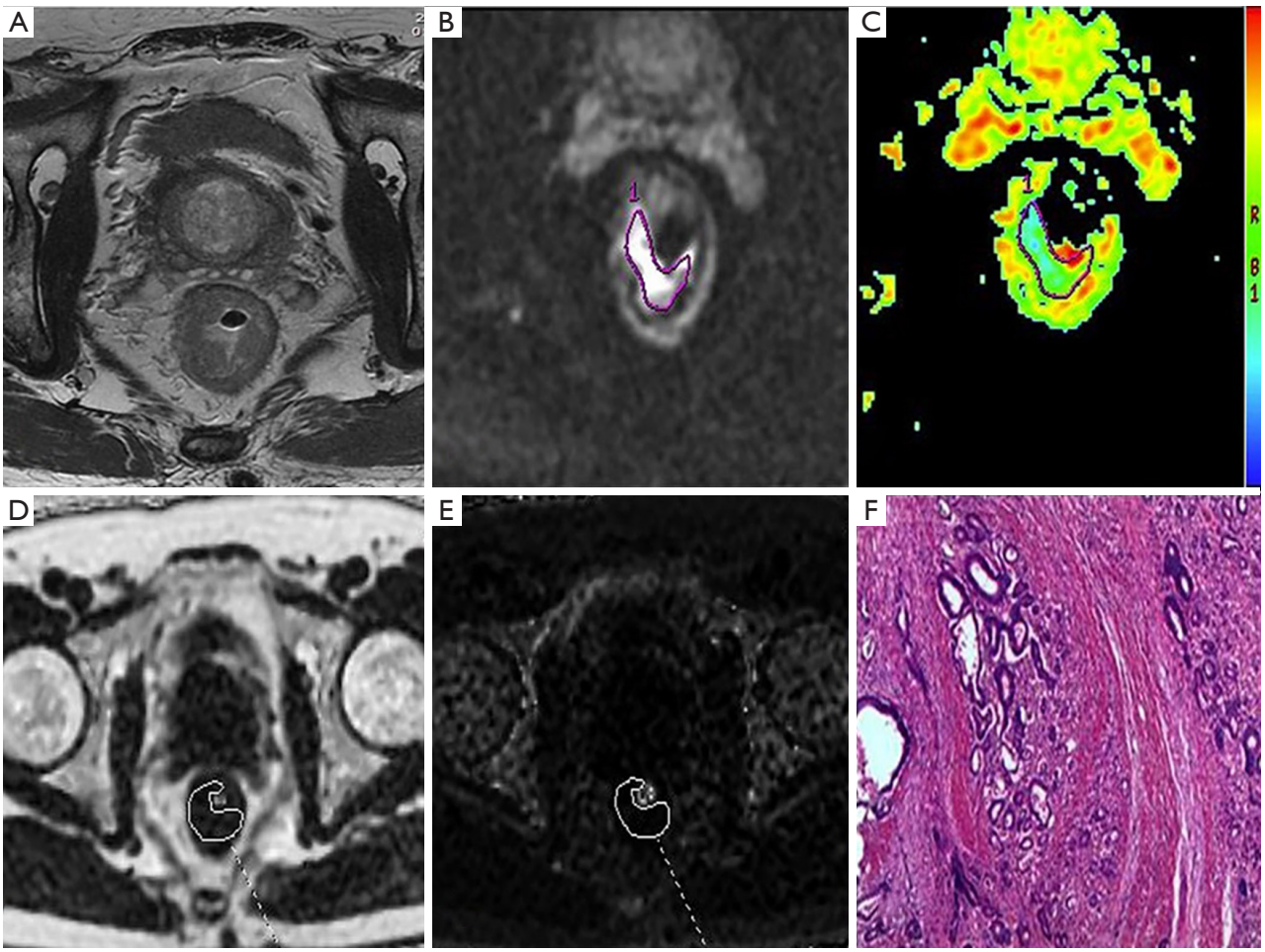

Figure 2 A 66-year-old male with stage T2 rectal adenocarcinoma (N1; moderately differentiated; EMVI+; MRF–). (A) Axial T2-weighted imaging demonstrates a moderately hyperintense mass in the rectum. (B) Axial diffusion-weighted imaging shows a mass with a heterogeneously high signal (restricted diffusion) in the rectal lumen. (C) The ADC color map (ADC =1.187×10^{-3} mm^2). (D) The PDFF map with delineation of corresponding rectal tumor (PDFF =3.22%). (E) The R2* map with delineation of corresponding rectal tumor (R2* =28.07 s^{-1}). (F) Histopathological HE staining (100×) revealing that the tumor had invaded the muscularis propria layer of the rectal wall. EMVI, extramural vascular invasion; MRF, mesorectal fascia; ADC, apparent diffusion coefficient; PDFF, proton density fat fraction; HE, hematoxylin and eosin.

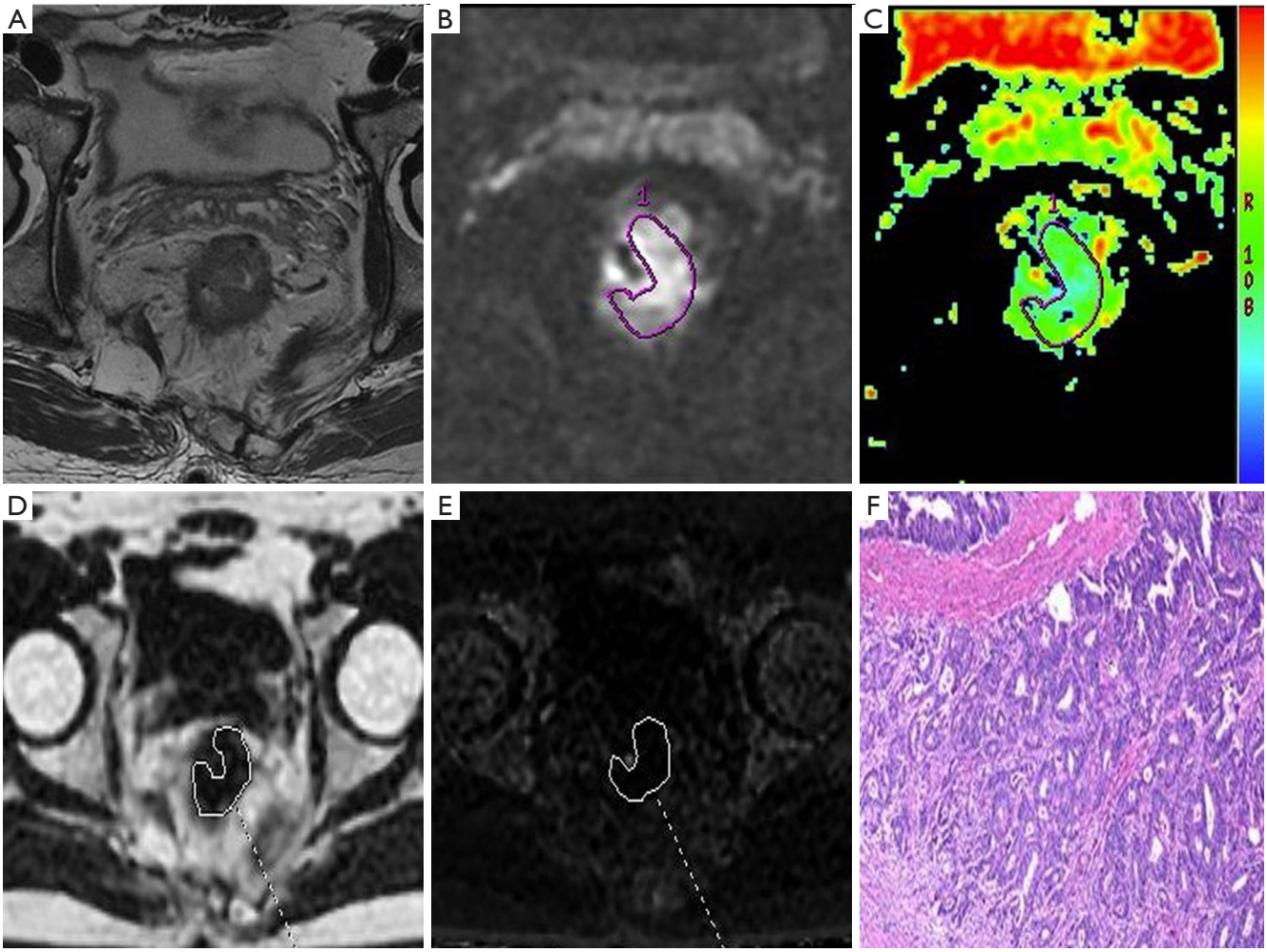

Figure 3 A 64-year-old male with T3 stage rectal adenocarcinoma (N0; poorly differentiated; EMVI+; MRF–). (A) Axial T2-weighted imaging demonstrates a moderately hyperintense mass in the rectum. (B) Axial diffusion-weighted imaging reveals a mass with a heterogenous high signal (restricted diffusion) in the rectal lumen. (C) The ADC color map (ADC =1.014×10^{-3} mm^2). (D) The PDFF map with delineation of corresponding rectal tumor (PDFF =4.85%). (E) The R2* map with delineation of corresponding rectal tumor (R2* =30.58 s^{-1}). (F) Histopathological HE staining (100×) revealing that the tumor had invaded the surrounding adipose tissue of the rectum. EMVI, extramural vascular invasion; MRF, mesorectal fascia; ADC, apparent diffusion coefficient; PDFF, proton density fat fraction; HE, hematoxylin and eosin.

ICC values indicated excellent agreement between readers. Furthermore, an excellent and reliable interobserver agreement was noted in Bland-Altman analysis. The Bland-Altman plots for 2 readers are shown in *Figure 5*.

Discussion

This investigation used the CSE-MRI sequence to quantify the PDFF and R2* of patients with rectal adenocarcinoma and control participants. We also assessed the role of CSE-MRI and DWI-derived parameters to differentiate histopathological features of rectal adenocarcinoma, namely T stage, lymph node metastasis, tumor grade, MRF status, and EMVI status. This study was a preliminary study based on the CSE-MRI technique to measure the intratumoral fat and R2* of rectal adenocarcinoma and analyze their relationships with histopathological features of tumors. Our objective was to identify the value of intratumoral fat component and R2* from CSE-MRI in predicting the prognostic factors of rectal adenocarcinoma as compare to

Table 4 ROC analysis of CSE-MRI and DWI in discriminating different histological features of rectal adenocarcinoma

Factors/multi-parameters	AUC	Cutoff	Sensitivity (%)	Specificity (%)	Youden index	P value
pT category						
PDFF	0.969 (0.931–1.000)	4.70△	95.00	87.50	0.825	<0.001
R2*	0.938 (0.882–0.996)	31.85☆	95.00	79.20	0.742	<0.001
ADC	0.743 (0.614–0.873)	1.03▲	87.50	61.70	0.492	0.001
pN category						
PDFF	0.865 (0.788–0.942)	5.44△	87.50	75.00	0.625	<0.001
R2*	0.781 (0.682–0.880)	35.15☆	80.00	68.20	0.482	<0.001
ADC	0.611 (0.490–0.733)	1.06▲	54.50	70.00	0.245	0.080
Tumor grade						
PDFF	0.795 (0.686–0.903)	6.31△	60.00	89.80	0.498	<0.001
R2*	0.693 (0.573–0.813)	31.85☆	96.00	35.60	0.316	0.007
ADC	0.627 (0.497–0.758)	0.91▲	89.80	36.00	0.258	0.066
MRF						
PDFF	0.823 (0.736–0.911)	5.59△	95.50	66.10	0.616	<0.001
R2*	0.713 (0.595–0.830)	32.30☆	95.50	38.70	0.342	0.003
ADC	0.538 (0.404–0.671)	1.17▲	17.70	100.00	0.177	0.600
EMVI						
PDFF	0.835 (0.750–0.920)	5.48△	87.10	66.00	0.531	<0.001
R2*	0.740 (0.634–0.845)	32.30☆	96.80	45.30	0.421	<0.001
ADC	0.607 (0.480–0.735)	0.91▲	90.60	32.30	0.228	0.102

△, the unit of the cutoff value for PDFF was %; ☆, the unit of the cutoff value for R2* was s^{-1}; ▲, the unit of the cutoff value for ADC was 10^{-3} mm^2/s. CSE-MRI, chemical shift–encoded magnetic resonance imaging; DWI, diffusion-weighted imaging; PDFF, proton density fat fraction; ADC, apparent diffusion coefficient; MRF, mesorectal fascia; EMVI, extramural vascular invasion; ROC, receiver operating characteristic curve; AUC, area under the curve.

that of DWI.

In our study, the interreader reproducibility analysis of CSE-MRI and DWI-derived parameters indicated excellent agreement between 2 independent readers, regardless of years of experience. These results showed that the measurements of PDFF, R2*, and DWI were reader-independent, and CSE-MRI imaging might be a practical and reproducible tool for the assessment of rectal adenocarcinoma.

We further found that PDFF and R2* values of patients with rectal adenocarcinoma were significantly lower than those of control participants. As previously reported, rectal adenocarcinoma is mainly composed of tubular or glandular structures and is poor in adipose tissue. As for the normal rectum, a certain amount of adipose tissue is contained in the submucosal and serosal layers of the rectum, including the epiploic appendices, which is the reason for the significantly higher PDFF values in control participants than in patients with rectal adenocarcinoma. A previous study found that the R2* parameter was influenced the paramagnetic deoxyhemoglobin concentration, oxygen status of tissues with microvessels, and blood flow (12). Higher R2* values were found in the normal rectum of control participants than in the afflicted rectum of those with rectal adenocarcinoma. This finding could be explained by the different tissue structures, vascular perfusion status, and paramagnetic deoxyhemoglobin concentrations in relation to various distributions of microvessels.

Higher PDFF and R2* values were noted in rectal adenocarcinoma with more aggressive histopathological

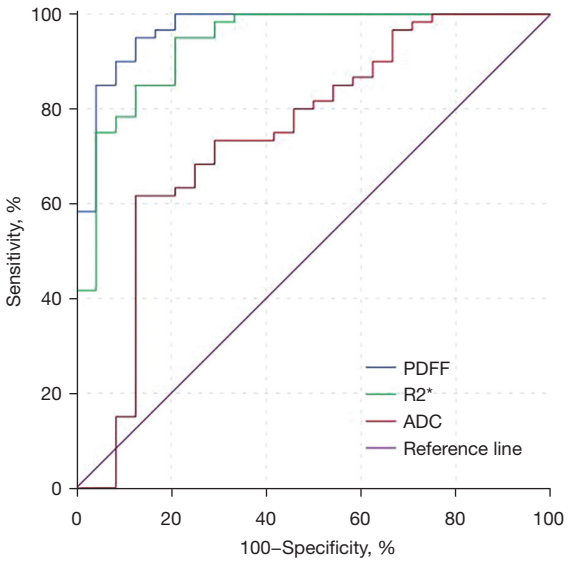

Figure 4 The diagnostic performance of CSE-MRI and DWI for distinguishing the T2 from the T3+T4 stages of rectal adenocarcinoma. CSE-MRI, chemical shift–encoded magnetic resonance imaging; DWI, diffusion-weighted imaging; PDFF, proton density fat fraction; ADC, apparent diffusion coefficient.

features, such as more advanced T stage, lymph node metastasis, high tumor grade, and MRF/EMVI invasion. MRF and EMVI are 2 independent prognostic factors of rectal adenocarcinoma for tumor recurrence and distant metastasis other than TNM categories (24,25). Adipose tissue was reported to be an important contributor to innate immune response mainly via cytokine/adipokine secretion, which ultimately leads to hyperplasia, proliferation, and carcinogenesis of colorectal cells (26). Especially in the tumor microenvironment, adipocytes and adipokines from adipose tissue can facilitate colorectal carcinogenesis and tumor development (27). Furthermore, adipose tissue–related angiogenesis might also contribute to the higher T stage, nodal involvement, higher tumor grade, and MRF/EMVI-positive status of rectal adenocarcinoma. Adipose tissue could modulate the angiogenic process and participate in tumor progression through signaling molecules (28,29). Tumor growth, progression, and distant metastasis are closely intertwined with angiogenesis (30). Previous studies have demonstrated that angiogenesis correlates with lymph node involvement, distant metastasis, and poor overall survival (31,32). The mutual interaction between adipose

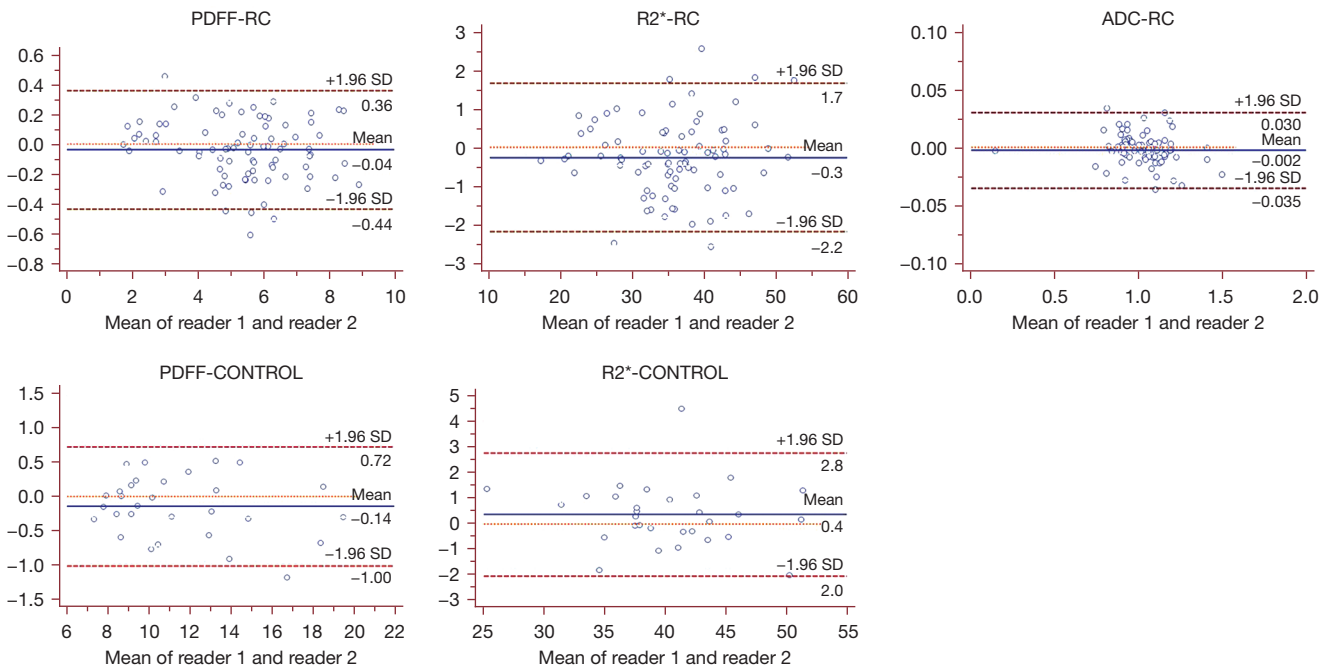

Figure 5 Bland–Altman analysis of CSE-MRI and DWI of patients with rectal cancer and control participants by 2 readers. PDFF, proton density fat fraction; RC, rectal cancer; CSE-MRI, chemical shift–encoded magnetic resonance imaging; DWI, diffusion-weighted imaging; ADC, apparent diffusion coefficient.

tissue and angiogenesis could further aggravate tumor proliferation and progression. Hence, we hypothesize that intratumoral adipose tissue could potentially facilitate the proliferation of tumor cells and progression in the tumor microenvironment of rectal adenocarcinoma.

With regard to the R2* parameter of CSE-MRI imaging, a higher R2* value was associated with a higher T/N stage, tumor grade, and MRF/EMVI-positive status. R2* has been found to reflect the liver iron content and tumor hypoxia of breast cancer (33,34). Previous reported (14,15) demonstrated that R2* correlated with the status of deoxyhemoglobin and blood oxygenation, with the increased level of blood deoxyhemoglobin could potentially leading to elevated R2* (35). Tumors with advanced stage lead to a more hypoxic microenvironment due to the rapid proliferation of tumor cells and tumor development (36,37), resulting in increased content of deoxyhemoglobin and R2* values. Meanwhile, tumor hypoxia further leads to angiogenesis, contributing to progression and distant metastasis (38). These factors could be the reasons for higher R2* values in patients with rectal adenocarcinoma and advanced T stage, nodal involvement, high tumor grade, and positive MRF/EMVI status.

The abilities of mean ADC and DWI to differentiate the T stage of rectal adenocarcinoma were significantly different. Mean ADC can quantify the magnitude of water molecule diffusion within tumor tissues. In one study, lower ADC values were associated with more aggressive tumors by virtue of the cytoplasmic protein/viscosity and nuclear size (39). No significant results were found concerning the ability of ADC to distinguish other histopathological features. This finding might be influenced by the single *b* value used, field intensity, and MR equipment with different vendors (40).

We studied the diagnostic abilities of CSE-MRI and DWI to predict the prognosis-related histopathological factors of rectal adenocarcinoma. The ROC analysis indicated PDFF and R2* had a better diagnostic performance than did ADC in discriminating some of the histopathological features. ADC is easily influenced by tumor microcirculation perfusion and motion artifacts. Different *b* values might lead to a bias in ADC values. From our investigation, the CSE-MRI sequence could provide a better diagnostic ability and additional information for the assessment of histopathological features of rectal adenocarcinoma.

Our study had some limitations. First, the study sample size was relatively small, and inevitable selection bias was inevitable. Second, the CSE-MRI imaging acquisition was highly dependent upon the homogeneity of the local magnetic field intensity. The intraluminal gas and bowel movement might lead to a heterogeneity of the magnetic field intensity and affect the measurements of CSE-MRI parameters, although racanisodamine hydrochloride was used to reduce bowel movement for patients with rectal cancer. Third, this investigation mainly focused on the relationships between CSE-MRI parameters and some prognostic factors of rectal adenocarcinoma. More prognosis-related factors should be taken into consideration. Moreover, factors related to clinical outcomes, including disease-free survival and overall survival rate, should also be included in future investigations. Fourth, this investigation was performed on patients with rectal cancer without a prior validation study. A validation study is essential for the analysis of the accuracy of this technique in assessing the histopathological fat and iron and may be completed in a future study using resected specimens. Fifth, the ROI for PDFF mapping unavoidably contained native subserosal fat tissue of the rectal wall for T3 and T4 stage rectal cancer, which might have influenced the value of PDFF. Finally, patients with rectal adenocarcinoma were selected for CSE-MRI imaging in our study without consideration of other histological types of rectal tumors, such as mucinous rectal adenocarcinoma, neuroendocrine tumor, and gastrointestinal stromal tumor. Further study is necessary to investigate the feasibility of using the CSE-MRI technique in different subtypes of rectal tumors.

In conclusion, the use of the CSE-MRI technique could feasibly characterize rectal cancer. The CSE-MRI technique was more effective and had a higher diagnostic efficacy than did ADC from DWI for the discrimination of histopathological factors of rectal adenocarcinoma.

Acknowledgments

Funding: This work was supported by the National Natural Science Foundation of China (Nos. 82071889, 82071890, 62131009, and 82102025).

Footnote

Reporting Checklist: The authors have completed the STARD reporting checklist. Available at https://qims.amegroups.com/article/view/10.21037/qims-22-879/rc

Conflicts of Interest: All authors have completed the ICMJE

uniform disclosure form (available at https://qims.amegroups.com/article/view/10.21037/qims-22-879/coif). The authors have no conflicts of interest to declare.

Ethical Statement: The authors are accountable for all aspects of the work in ensuring that questions related to the accuracy or integrity of any part of the work are appropriately investigated and resolved. The study conformed to the provisions of the Declaration of Helsinki (as revised in 2013). This study was approved by the Institutional Review Board of Tongji Hospital of Tongji Medical College of Huazhong University of Science and Technology, and informed consent for this retrospective study was waived.

References

1. Hashmi AA, Hashmi SK, Ali N, Thara K, Ali R, Edhi MM, Faridi N, Khan A. Clinicopathologic features of colorectal carcinoma: features predicting higher T-stage and nodal metastasis. BMC Res Notes 2018;11:52.
2. Jankowski M, Pietrzak L, Rupiński M, Michalski W, Hołdakowska A, Paciorek K, et al. Watch-and-wait strategy in rectal cancer: Is there a tumour size limit? Results from two pooled prospective studies. Radiother Oncol 2021;160:229-35.
3. Schaap DP, Voogt ELK, Burger JWA, Cnossen JS, Creemers GM, van Lijnschoten I, Nieuwenhuijzen GAP, Rutten HJT, Daniels-Gooszen AW, Nederend J, Kusters M. Prognostic Implications of MRI-Detected EMVI and Tumor Deposits and Their Response to Neoadjuvant Therapy in cT3 and cT4 Rectal Cancer. Int J Radiat Oncol Biol Phys 2021;111:816-25.
4. Ma L, Lian S, Liu H, Meng T, Zeng W, Zhong R, Zhong L, Xie C. Diagnostic performance of synthetic magnetic resonance imaging in the prognostic evaluation of rectal cancer. Quant Imaging Med Surg 2022;12:3580-91.
5. Hu S, Xing X, Liu J, Liu X, Li J, Jin W, Li S, Yan Y, Teng D, Liu B, Wang Y, Xu B, Du X. Correlation between apparent diffusion coefficient and tumor-stroma ratio in hybrid (18) F-FDG PET/MRI: preliminary results of a rectal cancer cohort study. Quant Imaging Med Surg 2022;12:4213-25.
6. Liesenfeld DB, Grapov D, Fahrmann JF, Salou M, Scherer D, Toth R, Habermann N, Böhm J, Schrotz-King P, Gigic B, Schneider M, Ulrich A, Herpel E, Schirmacher P, Fiehn O, Lampe JW, Ulrich CM. Metabolomics and transcriptomics identify pathway differences between visceral and subcutaneous adipose tissue in colorectal cancer patients: the ColoCare study. Am J Clin Nutr 2015;102:433-43.
7. Holowatyj AN, Haffa M, Lin T, Scherer D, Gigic B, Ose J, et al. Multi-omics Analysis Reveals Adipose-tumor Crosstalk in Patients with Colorectal Cancer. Cancer Prev Res (Phila) 2020;13:817-28.
8. Haffa M, Holowatyj AN, Kratz M, Toth R, Benner A, Gigic B, et al. Transcriptome Profiling of Adipose Tissue Reveals Depot-Specific Metabolic Alterations Among Patients with Colorectal Cancer. J Clin Endocrinol Metab 2019;104:5225-37.
9. Nieman KM, Romero IL, Van Houten B, Lengyel E. Adipose tissue and adipocytes support tumorigenesis and metastasis. Biochim Biophys Acta 2013;1831:1533-41.
10. Amemori S, Ootani A, Aoki S, Fujise T, Shimoda R, Kakimoto T, Shiraishi R, Sakata Y, Tsunada S, Iwakiri R, Fujimoto K. Adipocytes and preadipocytes promote the proliferation of colon cancer cells in vitro. Am J Physiol Gastrointest Liver Physiol 2007;292:G923-9.
11. Reeder SB, Wen Z, Yu H, Pineda AR, Gold GE, Markl M, Pelc NJ. Multicoil Dixon chemical species separation with an iterative least-squares estimation method. Magn Reson Med 2004;51:35-45.
12. Tang A, Tan J, Sun M, Hamilton G, Bydder M, Wolfson T, Gamst AC, Middleton M, Brunt EM, Loomba R, Lavine JE, Schwimmer JB, Sirlin CB. Nonalcoholic fatty liver disease: MR imaging of liver proton density fat fraction to assess hepatic steatosis. Radiology 2013;267:422-31.
13. Eskreis-Winkler S, Corrias G, Monti S, Zheng J, Capanu M, Krebs S, Fung M, Reeder S, Mannelli L. IDEAL-IQ in an oncologic population: meeting the challenge of concomitant liver fat and liver iron. Cancer Imaging 2018;18:51.
14. Miyata M, Aoki T, Shimajiri S, Matsuyama A, Kinoshita S, Fujii M, Katsuki T, Inoue Y, Nagata Y, Tashima Y, Korogi Y. Evaluation of the R2* value in invasive ductal carcinoma with respect to hypoxic-related prognostic factors using iterative decomposition of water and fat with

echo asymmetry and least-squares emission (IDEAL). Eur Radiol 2017;27:4316-23.
15. Peng Y, Luo Y, Hu X, Shen Y, Hu D, Li Z, Kamel I. Quantitative T2*-Weighted Imaging and Reduced Field-of-View Diffusion-Weighted Imaging of Rectal Cancer: Correlation of R2* and Apparent Diffusion Coefficient With Histopathological Prognostic Factors. Front Oncol 2021;11:670156.
16. Lee J, Kim CK, Gu KW, Park W. Value of blood oxygenation level-dependent MRI for predicting clinical outcomes in uterine cervical cancer treated with concurrent chemoradiotherapy. Eur Radiol 2019;29:6256-65.
17. Ge YX, Hu SD, Wang Z, Guan RP, Zhou XY, Gao QZ, Yan G. Feasibility and reproducibility of T2 mapping and DWI for identifying malignant lymph nodes in rectal cancer. Eur Radiol 2021;31:3347-54.
18. Li L, Chen W, Yan Z, Feng J, Hu S, Liu B, Liu X. Comparative Analysis of Amide Proton Transfer MRI and Diffusion-Weighted Imaging in Assessing p53 and Ki-67 Expression of Rectal Adenocarcinoma. J Magn Reson Imaging 2020;52:1487-96.
19. Curvo-Semedo L, Lambregts DM, Maas M, Beets GL, Caseiro-Alves F, Beets-Tan RG. Diffusion-weighted MRI in rectal cancer: apparent diffusion coefficient as a potential noninvasive marker of tumor aggressiveness. J Magn Reson Imaging 2012;35:1365-71.
20. Akashi M, Nakahusa Y, Yakabe T, Egashira Y, Koga Y, Sumi K, Noshiro H, Irie H, Tokunaga O, Miyazaki K. Assessment of aggressiveness of rectal cancer using 3-T MRI: correlation between the apparent diffusion coefficient as a potential imaging biomarker and histologic prognostic factors. Acta Radiol 2014;55:524-31.
21. Elmi A, Hedgire SS, Covarrubias D, Abtahi SM, Hahn PF, Harisinghani M. Apparent diffusion coefficient as a non-invasive predictor of treatment response and recurrence in locally advanced rectal cancer. Clin Radiol 2013;68:e524-31.
22. Park JY, Shin HJ, Shin KC, Sung YS, Choi WJ, Chae EY, Cha JH, Kim HH. Comparison of readout segmented echo planar imaging (EPI) and EPI with reduced field-of-VIew diffusion-weighted imaging at 3t in patients with breast cancer. J Magn Reson Imaging 2015;42:1679-88.
23. Zhang XY, Wang S, Li XT, Wang YP, Shi YJ, Wang L, Wu AW, Sun YS. MRI of Extramural Venous Invasion in Locally Advanced Rectal Cancer: Relationship to Tumor Recurrence and Overall Survival. Radiology 2018;289:677-85.
24. Park MJ, Kim SH, Lee SJ, Jang KM, Rhim H. Locally advanced rectal cancer: added value of diffusion-weighted MR imaging for predicting tumor clearance of the mesorectal fascia after neoadjuvant chemotherapy and radiation therapy. Radiology 2011;260:771-80.
25. Betge J, Pollheimer MJ, Lindtner RA, Kornprat P, Schlemmer A, Rehak P, Vieth M, Hoefler G, Langner C. Intramural and extramural vascular invasion in colorectal cancer: prognostic significance and quality of pathology reporting. Cancer 2012;118:628-38.
26. Riondino S, Roselli M, Palmirotta R, Della-Morte D, Ferroni P, Guadagni F. Obesity and colorectal cancer: role of adipokines in tumor initiation and progression. World J Gastroenterol 2014;20:5177-90.
27. Ramos-Nino ME. The role of chronic inflammation in obesity-associated cancers. ISRN Oncol 2013;2013:697521.
28. Ribatti D, Annese T, Tamma R. Adipocytes, mast cells and angiogenesis. Rom J Morphol Embryol 2020;61:1051-6.
29. Chang ML, Yang Z, Yang SS. Roles of Adipokines in Digestive Diseases: Markers of Inflammation, Metabolic Alteration and Disease Progression. Int J Mol Sci 2020.
30. De Palma M, Biziato D, Petrova TV. Microenvironmental regulation of tumour angiogenesis. Nat Rev Cancer 2017;17:457-74.
31. Boedefeld WM 2nd, Bland KI, Heslin MJ. Recent insights into angiogenesis, apoptosis, invasion, and metastasis in colorectal carcinoma. Ann Surg Oncol 2003;10:839-51.
32. Royston D, Jackson DG. Mechanisms of lymphatic metastasis in human colorectal adenocarcinoma. J Pathol 2009;217:608-19.
33. Wells SA. Quantification of hepatic fat and iron with magnetic resonance imaging. Magn Reson Imaging Clin N Am 2014;22:397-416.
34. Liu M, Guo X, Wang S, Jin M, Wang Y, Li J, Liu J. BOLD-MRI of breast invasive ductal carcinoma: correlation of R2* value and the expression of HIF-1α. Eur Radiol 2013;23:3221-7.
35. González Hernando C, Esteban L, Cañas T, Van den Brule E, Pastrana M. The role of magnetic resonance imaging in oncology. Clin Transl Oncol 2010;12:606-13.
36. Lu X, Kang Y. Hypoxia and hypoxia-inducible factors: master regulators of metastasis. Clin Cancer Res 2010;16:5928-35.
37. Bousquet PA, Meltzer S, Sønstevold L, Esbensen Y, Dueland S, Flatmark K, Sitter B, Bathen TF, Seierstad T, Redalen KR, Eide L, Ree AH. Markers of Mitochondrial Metabolism in Tumor Hypoxia, Systemic Inflammation,

and Adverse Outcome of Rectal Cancer. Transl Oncol 2019;12:76-83.
38. Yeo DM, Oh SN, Jung CK, Lee MA, Oh ST, Rha SE, Jung SE, Byun JY, Gall P, Son Y. Correlation of dynamic contrast-enhanced MRI perfusion parameters with angiogenesis and biologic aggressiveness of rectal cancer: Preliminary results. J Magn Reson Imaging 2015;41:474-80.
39. Schurink NW, Lambregts DMJ, Beets-Tan RGH. Diffusion-weighted imaging in rectal cancer: current applications and future perspectives. Br J Radiol 2019;92:20180655.
40. Sun H, Xu Y, Song A, Shi K, Wang W. Intravoxel Incoherent Motion MRI of Rectal Cancer: Correlation of Diffusion and Perfusion Characteristics With Prognostic Tumor Markers. AJR Am J Roentgenol 2018;210:W139-47.

Cite this article as: Peng Y, Li J, Hu X, Shen Y, Hu D, Li Z, Kamel I. Assessing the histopathological features of rectal adenocarcinoma with chemical shift–encoded sequence (CSE)-MRI and diffusion-weighted imaging (DWI). Quant Imaging Med Surg 2023;13(5):3199-3212. doi: 10.21037/qims-22-879

